sciendo | Journal of Electrical Bioimpedance | JoEB bioimpedance.net

J Electr Bioimp, vol. 10, pp. 96-102, 2019
Received 17 Nov 2019 / published 31 Dec 2019
https://doi.org/10.2478/joeb-2019-0014

Narrowband array processing beamforming technique for electrical impedance tomography

Venkatratnam Chitturi [1,3] and Nagi Farrukh [2]

1. *Asia Pacific University of Technology and Innovation, TPM, Bukit Jalil, Malaysia*
2. *Department of Mechanical Engineering, UniTEN, Selangor, Malaysia*
3. *E-mail any correspondence to: cratnamhere@gmail.com*

Abstract

Electrical impedance tomography (EIT) has a large potential as a two dimensional imaging technique and is gaining attention among researchers across various fields of engineering. Beamforming techniques stem from the array signal processing field and is used for spatial filtering of array data to evaluate the location of objects. In this work the circular electrodes are treated as an array of sensors and beamforming technique is used to localize the object(s) in an electrical field. The conductivity distributions within a test tank is obtained by an EIT system in terms of electrode voltages. These voltages are then interpolated using elliptic partial differential equations. Finally, a narrowband beamformer detects the peak in the output response signal to localize the test object(s). Test results show that the beamforming technique can be used as a secondary method that may provide complementary information about accurate position of the test object(s) using an eight electrode EIT system. This method could possibly open new avenues for spatial EIT data filtering techniques with an understanding that the inverse problem is more likely considered here as a source localization algorithm instead as an image reconstruction algorithm.

Keywords: Array processing; beamforming, EIDORS, electrical impedance tomography; numerical methods; source localization.

Introduction

Electrical impedance tomography (EIT) systems generally use a certain number of electrodes, which are placed on a medium with equal spacing to surround the domain that is imaged. A constant, low frequency and low magnitude alternating current is injected to a pair of electrodes and the potential differences, which is the function of unspecified conductivity distribution are measured from the remaining non-current carrying electrodes. The internal conductivity or permittivity or resistivity distribution is calculated based on the set of voltage measurements corresponding to the injected current. This technique is safe, inexpensive, non-invasive, portable and suitable for continuous imaging. A good introduction to the EIT: methods, history and applications is summarized in [1]. Although there is the capability of EIT to be utilized in the medical field, it has some limitations due to which there is hesitancy in adopting it for routine medical diagnosis. One such major limitation is low spatial resolution.

Array processing techniques utilize an array of similar sensors, which are spatially separated to analyze the signals such as in radars, sonars, radio astronomy, satellite communications, direction finding, seismology etc. Early array processing techniques in medical applications include ultrasonic imaging [2] and EEG signal processing [3]. Both of these applications use the concept of beamforming whose performance depends on the number of arrays as well as on the size of the arrays [4].

The beamforming concept is based on receiving of the signals by each element of an antenna array. These signals contain both amplitude and phase information. The beamforming is further carried out by adding weight to these signals in order to adjust the amplitude and phase in a way that when combined together, they produce the required beam. The major advantage of the beamforming technique is its spatial discrimination of the signals within an array of sensors. Amplitude tampering is typically applied to get a beam-shaped output where the main lobe contains the

information of interest [5]. Traditionally, there are narrowband beamformers and wideband beamformers. A narrowband beamformer is used in this study.

Applications of beamforming techniques for medical diagnosis include, a wideband beamformer in which multi frequency array processing is achieved by capturing the wide band frequency signal with a time delay signal. An ultra-wide band (UWB) beamformer was used to detect early breast tumors, using microwave technology. In such a beamformer, every antenna in the array emits an ultra-wide band (UWB) signal into the breast and in return receives the backscattered signals. After all the antennas have done their emissions, the responses are collected to generate a beamformer output. For the presence of a tumor, the beamformer output shows up a large energy signal. Thus the signal as a function of location provides an image. However, neither the shape nor the size of the tumor is known and further analysis is required [6]. Space-time beamforming techniques are simple in computation and effective. However, it lacks to image details of conductivity or permittivity or resistivity. Instead, an image of the variance of energy is displayed [7].

In another work, beamforming was used to reconstruct the image of the abnormalities of the breast. Photo acoustic technique, which combines the features of optical absorption and low dispersion feature of ultrasound, was used for the intended study. The breast was exposed with a Nd:YAG laser for a duration of 5 ns at 10 Hz. The propagated signals through the breast is then recorded by an ultrasound detector. The delay-and-sum beamforming algorithm was used to detect the peak-to-peak values of the signal, which are then added up for a selected portion of the breast. The highest peak-to-peak value would indicate the abnormalities in the breast [8]. Tumor localization was done using optical tomography and beamforming. The test object was divided into smaller regions called voxels. A beamformer was then designed based on linearly constrained minimum variance (LCMV) algorithm and was applied to each voxel. Tumors were localized in the form of peaks in the output signal. This method improved the spatial resolution, which got affected with an increase in the noise levels [9].

Beamforming technique was also proposed for the study of impedance changes as a function of time (temporal resolution). Prior computed tomographic (CT) images were used as a reference set in order to identify the regions of interest (ROI) of the object. Then, the impedance change was studied at different excitation frequencies (spectroscopy) [10]. Finally, beamforming technique was introduced to the EIT systems in order to study the conductivity changes. LCMV algorithm was adapted to accurately localize these conductivity changes. The current was injected to a pair of electrodes while the voltage difference was measured from the remaining pair of electrodes. In spite of simpler computations, the noise effect was a major drawback in this system [11].

So far, EIT has shown significant results as a functional imaging tool such as in continuous monitoring of cardiac functioning, lung functioning, etc. [12]. However, it is not fully suitable for anatomical imaging because of its poor spatial resolution. In this paper, we introduce the concept of array processing narrowband beamforming technique into the EIT systems mainly to improve the spatial resolution of the EIT images. This technique has been simulated and experimentally verified with an EIT system and would open new avenues for spatial EIT data filtering techniques and hence could be used to aid the inverse problems of the current EIT systems.

Materials and methods

This section discusses on the implementation of the numerical methods for the proposed study, the prototype of the actual EIT system and algorithms used.

Numerical Methods

Elliptic partial differential equations (PDEs) typically characterize boundary value problems with steady state conditions in two dimensions and hence can be employed to characterize the spatial distribution of an electrostatic field potential in EIT systems. The distribution of an electric potential within an object through which a steady current flows, can be represented by the solution of Poisson's equation, that reduces to Laplace's equation for a source free, homogeneous medium. The numerical solution for such elliptic PDEs is based on treating the test object as a grid of discrete points or *nodes* and transforming these PDEs into an algebraic finite difference equations [13].

The interior nodes are represented in terms of the Laplacian difference equations. The boundary conditions must be specified in order to obtain a unique solution. There would be more linear algebraic equations depending on the number of interior nodes. However, there would be a maximum of five (5) unknowns for each node (equation). For a large sized grids, this means that a significant number of terms would be zero. This could lead to the wastage of computer memory in storing zero's when full matrix elimination methods are used. Hence, approximation methods are used for obtaining the solutions for elliptical equations.

The numerical solution is provided by the most commonly used Gauss-Seidal method which when applied to partial differential equations, is referred to as Liebmann's method [11]. The matrix obtained is diagonally dominant and hence would converge on to a stable solution. The iterations are repeated until the absolute values of all the percentage relative errors (ε_a) fall below a specified stopping criteria, ε_s (usually 1%). The percentage relative errors are estimated by equation (1).

$$\left|(\varepsilon_a)\right| = \left|\frac{V(new) - V(old)}{V(new)}\right| \times 100\% \qquad (1)$$

Prototype of the actual EIT system

The block diagram of the developed beamforming EIT system is shown in Fig. 1. We assume that the currents do not flow in a straight line, instead, follow a path of higher conductivity regions. Also, the contact impedance issues are not considered in the study.

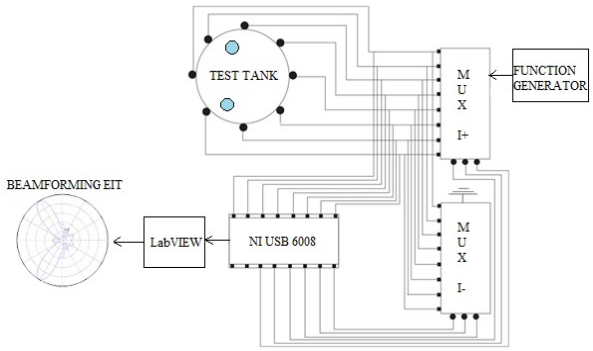

Fig. 1: Complete block diagram of the developed beamforming EIT system. The input current is injected into the electrodes adjacently through the multiplexer circuit. The individual voltages are measured by NI USB 6008 from the non-current carrying electrodes. The beamforming algorithm displays the location of the test objects in the form of two beams.

A recyclable, polyethylene terephthalate (PET) circular container of around 11 cm in diameter and 16 cm in height was used for the proposed study. Eight holes at every 4.4 cm were drilled along the circumference of the container and 6 cm from the bottom of the container. The holes were tightly sealed with the Ag/AgCl electrodes and then saline water (10% NaCl) of 12 cm height was filled in the container. A standard check was carried out by measuring the contact impedances of all the electrodes, which measured 0.6 Ω. Apart from that, the electrode considerations, excitation methods and voltage measurement techniques are according to [14].

CD4067BE is a single 16-channel multiplexer/demultiplexer IC. Only 8 channels were used for the intended study. (although only one IC was sufficient, two ICs were used for the possible extension of the number of electrodes to 16 in the future). These two multiplexers are used to perform the current injection into the test tank through the electrodes. One multiplexer is used for selecting the current source while the other multiplexer would select the ground. The signal from a function generator is injected into MUX I+ while MUX I- is connected to the ground. The function generator (Kikusui Electronics Corp, model 459) is used as a current source for the EIT system. The output current is determined by the output impedance and the output voltage.

With an output resistance of 600Ω and a maximum output voltage of 20 V_{PP}, a current of up to 33 mA could be generated. A safe let-go current of 6 mA [15] at 50 kHz is chosen as a mid-value from the optimum frequency range for electrical impedance tomography applications which is from 10 kHz to 100 kHz [16] for the proposed study.

The National Instruments, NI USB 6008 DAQ (data acquisition) card acquires the voltage data from the electrodes as well as acts as a control device for the multiplexers. The complete experimental set up of the EIT system using eight (8) electrodes is shown in Fig 2.

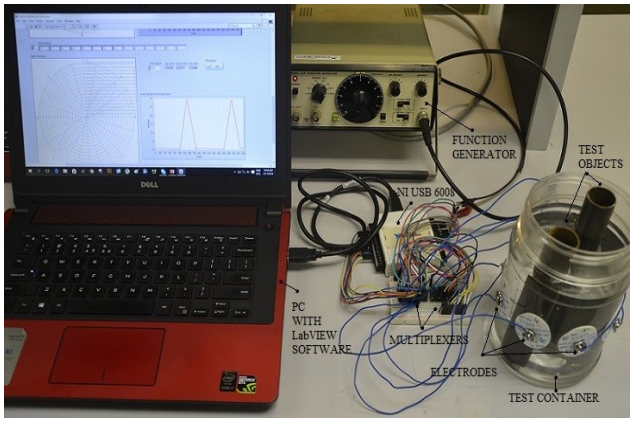

Fig. 2: Complete experimental set up of the proposed study. The test objects are placed at electrode positions 4 and 8 respectively. The beamforming algorithm locates the test objects in the form of two beams after acquiring the data from the EIT system with eight electrodes.

Algorithm Development

A program is developed to shift the currents according to a sequence using a multiplexer circuit. Two-electrode configuration is used where the input current is applied to a pair of electrodes, which would not measure any voltage readings. Thus, each electrode will have six analog voltages (rms values) for one cycle, as the other two readings will be zero during current injection. The program gets the sum of the individual electrode voltage readings after one complete cycle.

The Laplace equation for a circular test tank can be represented in the polar co-ordinates by equation (2), containing no free charges.

$$\frac{\partial^2 V}{\partial r^2} + \frac{\partial^2 V}{\partial \theta^2} = 0 \qquad (2)$$

where, r is the radius of the circle in centimeter and θ is the angle between two consecutive electrodes in radians.

Fig. 3 shows the circular test tank of radius r_1 for the intended EIT study. The test tank is insulated everywhere except at the points, where the electrodes, V_1-V_8, are connected, at an angular difference of 45 degrees. Also, the conductivity is assumed to be uniform inside the test tank.

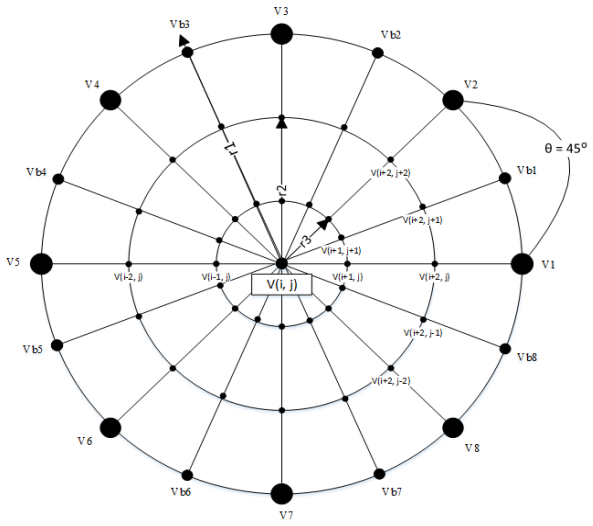

Fig. 3: A circular test tank of radius r_1. The radii of the two concentric circles are r_2 and r_3. Voltages V_1-V_8 are the measured electrode voltages. The electrodes are separated by an angle of θ=45 degrees. V_{b1}-V_{b8} are the voltages obtained from bi-curvilinear interpolation of V_1-V_8. The voltages $V_{(i,\ j)}$'s are the nodal voltages, which are derived from Gauss-Seidel method.

After acquiring the boundary electrode potentials, more boundary potentials are interpolated by bi-curvilinear interpolation given by equation (3), which are shown as V_{b1}-V_{b8} in Fig. 3.

$$V_{bk}(r,\theta) = \frac{V_2 V_{b1}}{V_2 V_1} \times V_1(r_1,\theta_1) + \frac{V_{b1} V_1}{V_2 V_1} \times V_2(r_2,\theta_2) \quad (3)$$

where, V_2V_{b1} and $V_{b1}V_1$ are arc lengths, k = 1…8, $r_1 = r_2$ and θ_1 = 22.5 degrees while θ_2 = 45 degrees.

Now for interpolating the internal nodal voltages, the circular test tank is treated as grids of discrete points as shown once again in Fig. 3. The central difference equations based on the grid scheme are given by equation (4) and equation (5).

$$\frac{\partial^2 V}{\partial r^2} = \frac{V_{i+1,j} - 2V_{i,j} + V_{i-1,j}}{\Delta r^2} \quad (4)$$

$$\frac{\partial^2 V}{\partial \theta^2} = \frac{V_{i,j+1} - 2V_{i,j} + V_{i,j-1}}{\Delta \theta^2} \quad (5)$$

The radius is taken as the first dimension while the arc length is considered instead of the angle, θ, (equation (6)) as the second dimension.

$$\frac{\partial^2 V}{\partial \theta^2} = \frac{V_{i,j+1} - 2V_{i,j} + V_{i,j-1}}{\Delta \cap^2} \quad (6)$$

Substituting equation (4) and equation (6) in equation (2),

$$\frac{V_{i+1,j} - 2V_{i,j} + V_{i-1,j}}{\Delta r^2} + \frac{V_{i,j+1} - 2V_{i,j} + V_{i,j+1}}{\Delta \cap^2} = 0 \quad (7)$$

Equation (7) is the Laplacian difference equation for the interior nodal voltages. Assuming, $\Delta r = \Delta \cap = h$, the matrix structure of the five-point approximation can be represented as,

$$\begin{pmatrix} 0 & 1 & 0 \\ 1 & -4 & 1 \\ 0 & 1 & 0 \end{pmatrix} \begin{pmatrix} * & V_{i,j+1} & * \\ V_{i-1,j} & V_{i,j} & V_{i+1,j} \\ * & V_{i,j-1} & * \end{pmatrix} = h^2$$

The boundary potentials must be specified in order to obtain a unique solution. Laplacian difference equations are developed for each interior nodal voltage, which result in an 'n', number of simultaneous equations with (n-1) unknowns ($V_{(i,\ j)}$, the central voltage is assumed as the average of the measured boundary voltages for a homogeneous saline region). For any other value(s), the electrostatic potential distribution would be misleading). The numerical solution for the above Laplacian difference equations are obtained as discussed in numerical methods section. The rate of convergence can be further accelerated using over-relaxation methods [17].

A time difference approach is used to locate the test objects. Initially, a set of voltage readings is taken of the empty saline tank as a reference frame. Later, a second set of voltage readings are taken with the test object inside the test tank. Finally, the difference of the voltage readings of the two sets is fed as the boundary voltages. After the above interpolations, the concept of narrowband beamformer is applied where all the voltage values are summed up w.r.t. a particular angle. A test object is detected as a peak in the output voltage signal. Finally, suitable weight (a multiplication factor) is chosen independent of the electrode data for the accurate representation of the test object along its radius.

The test tank is filled with saline (10% NaCl) water for better conductivity. An eight electrode EIT system is considered for the simplicity of the design. A current of 6 mA at 50 kHz is injected adjacently w.r.t. ground. In return, the raw mono-polar voltages (assuming the noise levels to be negligible in the measured data, high SNR) are measured from the remaining non-current carrying electrodes in a cyclic manner which are later summed up for successive current patterns in a single measurement cycle. The basic image reconstruction of EIDORS [18] is considered for the comparison of the reconstructed images. A test object in the form of a hollow cylindrical iron rod was used. The dimensions include 15.5 cm length and 2.5 cm diameter. The test object(s) would be placed in line with the electrodes and then in the vicinity of the electrodes.

Ethical approval

The conducted research is not related to either human or animal use.

Results

Test objects placed in line with electrodes

When a single test rod is placed exactly in line with the electrode locations (not touching the electrodes), the conventional EIDORS gives distorted images due to contact impedance issues. On the other hand, the beamforming algorithm shows the exact location of the test object. A peak output in the beamforming represents the location of the test object as shown in Fig. 4. Hence, the beamforming algorithm is good for detection.

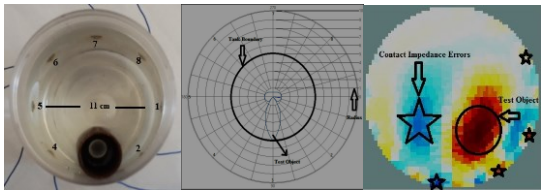

(a) (b) (c)

Fig. 4: (a) = actual test object placed along the line of electrode 1, (b) = test object as located using beamforming algorithm. A thick circle represents the actual diameter of the test tank and (c) = test object as indicated by EIDORS. The circle represents the actual object while the stars indicate the contact impedance errors.

Similar results are visible as compiled in Fig. 5 for different locations of the test object with the same considerations.

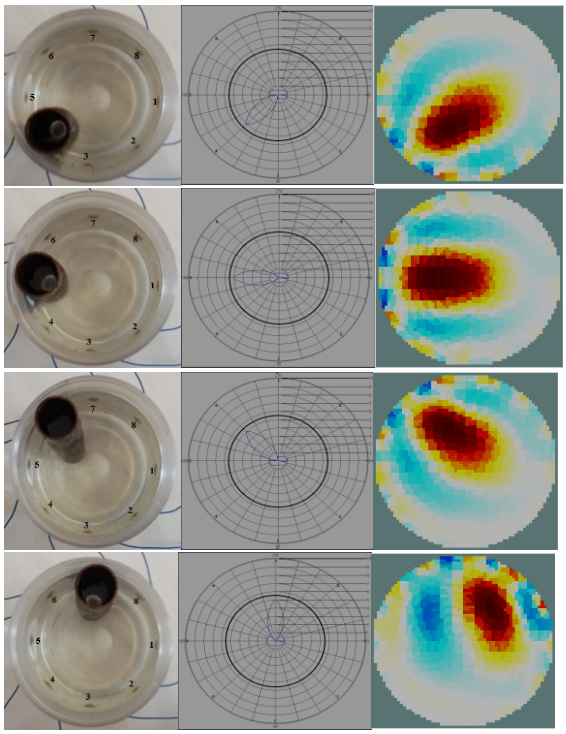

Fig. 5: Compiled one object test results for different locations.

Similarly, when two cylindrical test rods of same material and same dimensions were placed in the test tank, once again exactly in line with the electrode positions, EIDORS had the same contact impedance issues. While, the beamforming algorithm showed the exact locations of the test objects as seen in Fig. 6. Hence, the beamforming is good for distinguishability.

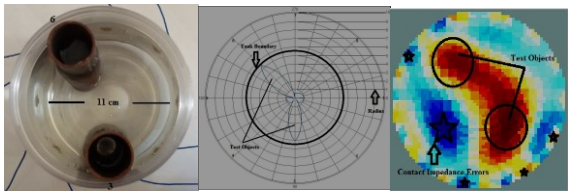

(a) (b) (c)

Fig. 6: (a) = actual test objects placed along the line of electrode 3 and electrode 6 respectively, (b) = test objects as located using beamforming algorithm. A thick circle represents the actual diameter of the test tank and (c) = test objects as indicated by EIDORS. The circle represents the actual object while the stars indicate the contact impedance errors.

Similar results are visible as compiled in Fig. 7 for the two test objects in different locations with the same considerations.

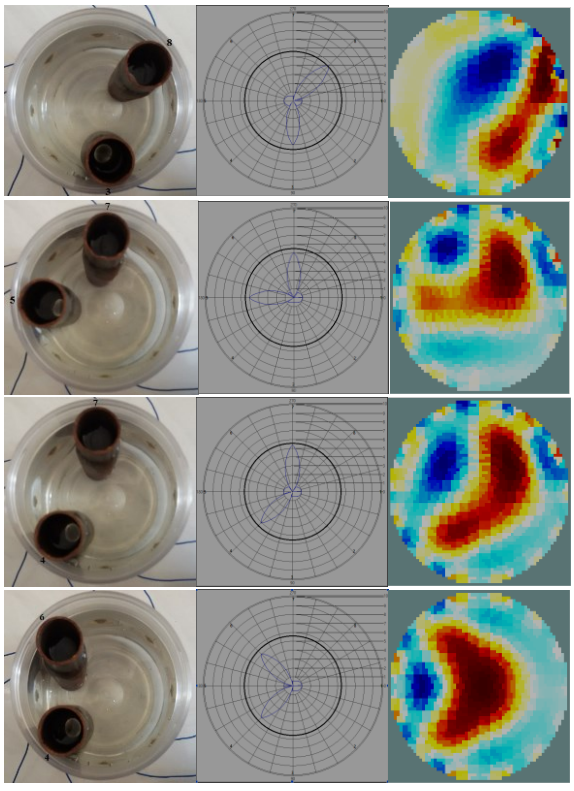

Figure 7: Compiled two object test results for different locations.

Test objects placed in the vicinity of the electrodes

However, when a test object is placed between two electrode positions, the beamforming shows a flat response running across the two electrodes instead of showing a peak in between the two electrodes as seen in Fig. 8(a). This is due

to the similar voltage drops captured by the two electrodes when the test object is placed between them. The same condition is also visible with two test objects placed between any two electrodes as shown in Fig. 8(b).

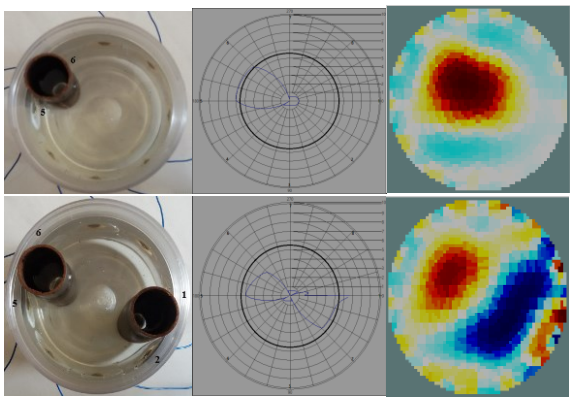

Fig. 8: (a) A single test object placed between electrode positions 5 and 6 (top). Two test objects placed between electrode positions 1-2 and 5-6 (bottom). (b) The beamforming algorithm gives a flat beam across electrode positions 5 and 6 (top) and a flat beam across electrode positions 1-2 and 5-6 (bottom). (c) EIDORS results for the given locations of the test objects.

The problem of flat beam response can be solved by using more electrodes in order to indicate the exact location(s) of the test object(s). Even three test objects could be detected exactly by the beamforming algorithm when placed exactly along the electrode alignment. A maximum of four (4) test objects can be detected by the developed EIT system. For the test tank of 11 cm diameter with eight electrodes at every 4.4 cm along the circumference, a decent spatial resolution of 6.3 cm is achieved without a flat beam response.

However, the spatial resolution could be improved further by simply increasing the number of electrodes. For example, for the same test tank with 16 electrodes, the spatial resolution could be 3.15 cm and with 32 electrodes would be 1.575 cm and so on. But, there is a limit for increasing the number of electrodes beyond which the image resolution is no longer improved [19]. More electrodes also mean more hardware and hence more processing time. Moreover, if an EIT system uses a number of electrodes, then all the electrodes must be driven by the input currents simultaneously for better results [20].

All the test results show conductivity beam(s) when the test object(s) are placed in the vicinity of the electrodes (along the periphery). However, when placed in the middle of test tank, the beamforming (only the conductors were tested for the intended study) algorithm showed a flat beam. Moreover, there was no object detected by the system when the test objects were smaller than 1 cm in diameter. The numerical solutions discussed are limited to circular test objects. Hence, prior modeling of any other shapes is required for better images. Also, neither the shape nor the size of the test object can be known.

Therefore, there is place for improvement of the measurement system by the following ways: by decreasing the size and increasing the number of electrodes (at least up to 16), by applying the better electrode setup (e.g. four electrode configuration), in trying other current injection patterns; e.g., some current injection patterns such as opposite or polar driven pattern produce more field strength in deeper regions of the medium and in this way provide images with higher resolution, by using a central electrode for more accurate readings, by employing more advanced image reconstruction algorithms like time-difference algorithms using multi-frequency information [21] and/or deep learning beamforming algorithms [22], by employing numerical solutions which are not limited to circular objects, by considering the noise levels in the measured data due to EIT circuitry and also by considering the contact impedances issues.

All the above suggestions for improvement of the measurement system would contribute to decreasing the contact impedance, increasing the signal to noise ratio and hence increasing the spatial resolution of the EIT images. Thus, it is suggested that these would be taken into consideration for future perspectives in order to enable EIT as a common imaging modality

Conclusion

Overall, the basic EIDORS reconstruction algorithm do not show the exact location of the test objects probably due to the contact impedance issues. On the other hand, results that are more accurate are visible using the beamforming technique, which can readily cope up with the electrode errors. However, the proposed narrowband beamforming method only seems to deliver acceptable results for inclusions close to the boundary test object(s).

To summarize, tomographic images, especially functional tomographic images are quantitative and come up with non-linear inverse problems. While beamforming techniques are qualitative and are free from the inverse problems. Therefore, beamforming techniques can be used to solve the inverse problems [10]. However, we have considered the inverse problem more likely as a source localization algorithm instead of as an image reconstruction algorithm. Hence, beamforming technique can be used as a secondary method that may provide complementary information about accurate positions of conductivity perturbations in present EIT systems

Conflict of interest

Authors state no conflict of interest.

References

1. D. S. Holder, "Electrical Impedance Tomography: Methods, History and Applications", CRC Press, 2004.
2. S. Manohar, A. Kharine, J. C. G. van Hespen, W. Steenbergen, and T. G. van Leeuwen, “The Twente Photoacoustic Mammoscope: system overview and performance.,” Phys. Med. Biol., vol. 50, no. 11, pp. 2543–57, 2005. https://doi.org/10.1088/0031-9155/50/11/007
3. E. A. Thompson, J. Xiang, and Y. Wang, “Frequency-spatial beamformer for MEG source localization,” Biomed. Signal Process. Control, vol. 18, pp. 263–273, 2015. https://doi.org/10.1016/j.bspc.2015.01.004
4. M. Viberg, "Introduction to Array Processing", Academic Press Library in Signal Processing, vol. 3, pp. 463-502, 2014. https://doi.org/10.1016/B978-0-12-411597-2.00011-4
5. B. D. Van Veen and K. M. Buckley, “Beamforming: a versatile approach to spatial filtering,” IEEE ASSP Mag., vol. 5, no. April, pp. 4–24, 1988. https://doi.org/10.1109/53.665
6. E. J. Bond, X. Li, S. C. Hagness, and B. D. Van Veen, “Microwave imaging via space-time beamforming for early detection of breast cancer,” IEEE Trans. Antennas Propag., vol. 51, no. 8, pp. 1690–1705, 2003. https://doi.org/10.1109/tap.2003.815446
7. T. F. Zanoon and M. Z. Abdullah, “Early stage breast cancer detection by means of time-domain ultra-wide band sensing,” Meas. Sci. Technol., vol. 22, no. 11, p. 114016, 2011. https://doi.org/10.1088/0957-0233/22/11/114016
8. N. Cao and A. Nehorai, “Tumor localization using diffuse optical tomography and linearly constrained minimum variance beamforming,” vol. 15, no. 3, pp. 896–909, 2007. https://doi.org/10.1364/oe.15.000896
9. C. S. Lengsfeld and R. A. Shoureshi, “System and Method for Beamforming in Soft-Field Tomography,” US 2013/0109962 A1, 2008.
10. P. Lafortune and R. Aris, “Linearly constrained minimum variance spatial filtering for localization of conductivity changes in electrical impedance tomography,” Int. J. Numer. Method. Biomed. Eng., vol. 28, no. 1, pp. 72–86, 2015. https://doi.org/10.1002/cnm.2703
11. J. S. Lioumbas, A Chatzidafni, and T. D. Karapantsios, “Spatial considerations on electrical resistance tomography measurements,” Meas. Sci. Technol., vol. 25, no. 5, p. 055303 (12 pp.), 2014. https://doi.org/10.1088/0957-0233/25/5/055303
12. G. J. Saulnier, R. S. Blue, J. C. Newell, D. Isaacson, and P. M. Edic, “Electrical impedance tomography,” IEEE Signal Process. Mag., vol. 18, no. 6, pp. 31–43, 2001. https://doi.org/10.1109/79.962276
13. C. Venkatratnam and N. Farrukh, “A Novel Numerical Technique to Enhance the Spatial Resolution of Electrical Impedance Tomography Systems,” IJAER, vol. 10, no. 19, pp. 40659–40662, 2015.
14. C. Venkatratnam and N. Farrukh, “Electrode considerations, excitation methods and measurement techniques for electrical impedance tomography,” IFMBE Proc., vol. 56, pp. 1–5, 2016. https://doi.org/10.1007/978-981-10-0266-3_1
15. R. M. Fish and L. a Geddes, “Conduction of electrical current to and through the human body: a review.,” Eplasty, vol. 9, p. e44, 2009.
16. M. Sikora, Ryszard Zenczak, “Optimum selection of frequency for medical equipment using electrical impedance tomography,” Int. J. Appl. Electromagn. Mech., vol. 10, no. 2, pp. 130–153, 1999. https://doi.org/10.3233/jae-1999-136
17. S. C. Chapra and R. P. Canale, “Numerical methods for engineers,” Math. Comput. Simul., vol. 33, no. 3, p. 260, 2015.
18. Adler and W. R. B. Lionheart, “Uses and abuses of EIDORS: an extensible software base for EIT.,” Physiol. Meas., vol. 27, no. 5, pp. S25–S42, 2006. https://doi.org/10.1088/0967-3334/27/5/s03
19. C.-N. Huang, F.-M. Yu, and H.-Y. Chung, “Rotational electrical impedance tomography,” Meas. Sci. Technol., vol. 18, no. 9, pp. 2958–2966, 2007. https://doi.org/10.1088/0957-0233/18/9/028
20. J. C. N. Margaret, Cheney David, “Electrical Impedance Tomography,” SIAM Rev., vol. 41, no. 1, pp. 85–101, 1999.
21. Cao *et al.* "A novel time-difference electrical impedance tomography algorithm using multi-frequency information" BioMedical Engineering OnLine., vol. 18, 84, 2019.
22. Vedula *et al.* "Learning beamforming in ultrasound imaging" Proceedings of Machine Learning Research, vol. 102, pp.493–511, 2019.